Muon location and muon dynamics in DyNi5

Mulders, A.M.; Kaiser, C.T.; Harker, S.J.; Gubbens, P.C.M.; Amato, A.; Gygax, F.N.; Schenck, A.; de Reotier, P.D.; Yaouanc, A.; Buschow, K.H.J.; Menovsky, A.A.

[Link to publication](#)

Muon location and muon dynamics in DyNi$_5$

A. M. Mulders,[1,2] C. T. Kaiser,[1] S. J. Harker,[1] and P. C. M. Gubbens[1]

[1]*Interfacultair Reactor Instituut, Delft University of Technology, Mekelweg 15, 2629 JB Delft, The Netherlands*
[2]*School of Physics and Materials Engineering, Monash University, Clayton, VIC 3800, Australia*

A. Amato
Laboratory for Muon-Spin Spectroscopy, PSI, CH-5232 Villigen PSI, Switzerland

F. N. Gygax and A. Schenck
Institute for Particle Physics of ETH Zurich, CH-5232 Villigen PSI, Switzerland

P. Dalmas de Réotier and A. Yaouanc
Commissariat à l'Energie Atomique, Département de Recherche Fondamentale sur la Matière Condensée,
F-38054 Grenoble cedex 9, France

K. H. J. Buschow and A. A. Menovsky
Van der Waals−Zeeman Instituut, University of Amsterdam, Valckenierstraat 65, 1018 XE Amsterdam, The Netherlands

In DyNi$_5$, the muon localizes at the $6i$ (1/2,0,0.1) interstitial site and below ~ 80 K a second muon site becomes populated, the metastable 6_{ring} site. We determine the mean residence time of the muon in this ring site and analyze its temperature dependence with a multiphonon quantum diffusion process. The coincidence energy is measured to be $E_a/k_B = 400$ (20) K and the tunneling matrix element $J = 0.21$ (7) meV. A comparison with GdNi$_5$ gives insight in the muon potential well scheme in these compounds. We attribute the large diversity of muon sites in RNi$_5$ series, where R is a rare earth element, to the relatively low density of states at the Fermi level.

I. INTRODUCTION

A few years ago, an interesting muon hopping feature was discovered in GdNi$_5$.[1-3] At low temperatures the muon occupies two different sites of which one consists of a ring of six equivalent sites that are all occupied by the muon within the time scale of muon spectroscopy, that is 10^{-9} s. As the temperature is raised this muon ring site becomes unstable ($T > 40$ K) and the muon hops to the second and preferred muon site. At elevated temperatures ($T > 80$ K) only this latter site is occupied by the muon. The muon sites are identified as the 6_{ring} [(0,0.225,1/2) or (0.13,0.26,1/2)] and the $3f$ (1/2,0,0) site, respectively. The muon hopping from the 6_{ring} to the $3f$ site has been successfully described by an incoherent multiphonon tunneling process, where a large number of phonons are involved in the deformation of the muon surroundings allowing the muon to tunnel through the energy barrier that is separating both sites. Clear indications exist that this phenomenon also occurs in the isostructural compounds DyNi$_5$, ErNi$_5$, and TbNi$_5$.[1]

The formation of a muon ring site has also been observed in the structurally related UNi$_2$Al$_3$ (Ref. 4) and is suspected in the superconductor MgB$_2$.[5] In addition, this phenomenon has recently been observed in CeAl$_2$, which crystalizes in the $C15$ Laves phase structure.[6]

The muon sites observed in the RNi$_5$ series (R is a rare earth element) are diverse as is summarized in Table I. It is remarkable that no systematic trend across the R series is observed and that various $6i$ and $3f$ sites are seen.

In this paper we report on the muon site determination in DyNi$_5$. Muon hopping is unambiguously present and analyzed within the framework of incoherent multiphonon tunneling. A comparison with the results obtained previously on GdNi$_5$ demonstrates certain characteristics of the muon localization behavior and we discuss the irregular localization behavior of the muon across the RNi$_5$ series.

DyNi$_5$ crystallizes in the hexagonal CaCu$_5$ structure (see Fig. 1). Its magnetic properties are well described by crystal electric field theory. DyNi$_5$ is a planar ferrimagnet ($T_C = 12$ K) with ferromagnetically aligned Dy moments. A small moment of $0.39\mu_B$ is induced in the Ni $3d$ sublattice and the exchange coupling between the Dy and Ni moments is strong and negative.[8] At 2 K the Dy moments equal $8.9\mu_B$ and are aligned along the $\bar{a}$ axis, that is the hexagonal b axis. At 6 K a moment reorientation has been observed and the a axis becomes the easy axis.[12] The crystal field induced anisotropy is large and present up to room temperature.[8,13]

II. EXPERIMENTAL DETAILS

A single crystal of DyNi$_5$ was prepared by the Czochralski method in Amsterdam from starting materials of at least 99.99% purity. The sample has been cut into a spherical shape (diameter of 4.5 mm) with spark erosion and has been oriented using x-ray Laue diffraction with either the $\bar{a}$ or c axis parallel to the rotation axis of the sample holder.

The susceptibility of the spherical sample has been determined with a SQUID magnetometer at Melbourne for the

TABLE I. Material parameters and muon sites in $R\text{Ni}_5$ compounds. Lattice parameters a and c are all taken from Ref. 7. The $4f$ shell electronic configuration is given for each rare earth R. M_R and M_{Ni} are, respectively, the R and Ni magnetic moments. T_C is the Curie temperature. The magnetic properties are taken from Ref. 8, and references therein. Muon sites indicated with an asterisk are determined in this paper. For location of the various muon sites see Fig. 1.

R ion	a	c/a	M_R (μ_B)	M_{Ni} (μ_B)	Easy axis	T_C (K)	Muon site(s)	
La $4f^0$	5.014	0.794	0	0			$3f$ or $6i$*	$(\frac{1}{2},0,0)$ (Ref. 9) or $(\frac{1}{2},0,z)$ with $z\leq0.21$*
Pr $4f^2$	4.957	0.803	0	0			$6i$	$(\frac{1}{2},0,0.21)$ (Ref. 10)
Gd $4f^7$	4.906	0.808	7.0	0.16	c	32	$3f$ and 6_{ring}	$(\frac{1}{2},0,0)$ + ring site for $T<80$ K (Ref. 3)
Tb $4f^8$	4.894	0.810	7.9	0.088	a	23	? and 6^*_{ring}	two sites below ~60 K (Ref. 11)
Dy $4f^9$	4.872	0.815	8.9	0.078	b	12	$6i$* and 6^*_{ring}	$(\frac{1}{2},0,0.1)$ + ring site for $T<80$ K
Er $4f^{11}$	4.858	0.816	9.0	0.076	c	9	$3f$ and ?	$(\frac{1}{2},0,0)$ for $T>100$ K (Ref. 8)

three crystallographic directions. Additionally, magnetization curves have been obtained between 2 and 14 K with the crystallographic a and $\bar{a}$ direction of the crystal parallel to the external field. The μ^+SR transverse field (TF) measurements took place at the GPS beam line at the Paul Scherrer Institute (PSI). All TF μSR spectra were taken with $B_{\text{ext}} = 0.6$ T at temperatures between 15 and 270 K with the a and c axes parallel to the external field. In addition angular scans in the $a\bar{a}$ plane and ac plane have been taken. Zero-field spectra were also recorded in the ordered phase. All spectra show a small background due to muons stopping in the copper sample holder. This background signal is included in all fitting procedures.

III. BACKGROUND

The muon, which is a spin $\frac{1}{2}$ particle, localizes at an interstitial site in the host crystal lattice. If locally a magnetic induction $\mathbf{B}_{\text{loc}}$ is present the muon spin will precess with an angular frequency $\omega = \gamma_\mu B_{\text{loc}}$, where γ_μ is the gyromagnetic ratio of the muon, $\gamma_\mu = 851.6$ Mrad s^{-1} T^{-1}. The origin of $\mathbf{B}_{\text{loc}}$ can be either the magnetic ordering of the host atoms or

FIG. 1. Unit cell of DyNi$_5$ (hexagonal crystal structure, space group $P6/mmm$, lattice parameters $a=4.872$ Å and $c=3.956$ Å). The muon localizes at the $6i$ site in the whole temperature range and also below ~80 K in either the $6m$ $(0.13,0.26,\frac{1}{2})$ or $6k$ $(0.225,0,\frac{1}{2})$ sites. The muon occupies all latter six sites within the time range of the experiment. Similar work on UNi$_2$Al$_3$ (Ref. 4) suggests that the muon forms an extended localized ring-shaped orbit. We refer to this site as the 6_{ring} site.

due to an external field. In the latter case, the external field polarizes the electrons of the host and the muon spin experiences the sum of both fields. We consider DyNi$_5$ in its paramagnetic state and briefly summarize the experimental background. For a detailed description of this method see for example Refs. 15 and 16.

The relative shift in muon precession frequency $K^\alpha = (B_{\text{loc}}^\alpha - B_{\text{ext}})/B_{\text{ext}}$ along the α direction is generally written as

$$K^\alpha = K_0^\alpha + K_{4f}^\alpha, \tag{1}$$

where K_0^α is due to the Pauli paramagnetism of the itinerant electrons. It is small and commonly supposed to be temperature independent. The coupling between the $4f$ moments in the host and the muon at its interstitial site is largely of dipolar origin. In addition to this the muon experiences its nearest neighbor $4f$ moments via the exchange interaction that polarizes the conduction electrons

$$K_{4f}^\alpha = (A_{\text{dip}}^{\alpha\alpha} + A_{\text{con}})\chi_{4f}^\alpha \tag{2}$$

with

$$A_{\text{dip}}^{\alpha\gamma} = \frac{1}{4\pi} \sum_i^{\text{LS}} D_i^{\alpha\gamma},$$

where

$$D_i^{\alpha\gamma} = v_c \left(\frac{3r_i^\alpha r_i^\gamma}{r_i^5} - \frac{\delta^{\alpha\gamma}}{r_i^3} \right). \tag{3}$$

χ_{4f} is the $4f$ susceptibility which is approximately equal to the bulk susceptibility. $A_{\text{dip}}^{\alpha\gamma}$ is the sum of the dipolar interaction between the muon spin and the $4f$ moments restricted to atoms inside a Lorentz sphere. $\mathbf{r}_i$ is the vector distance between the muon and atom i, v_c is the volume of the crystallographic unit cell, and $\delta^{\alpha\gamma}$ the Kronecker symbol. The contact interaction A_{con} is understood to be isotropic and only the nearest-neighbor moments of the muon contribute to it.

As the experiment has been performed on a spherical crystal, the Lorentz field and the demagnetization field at the
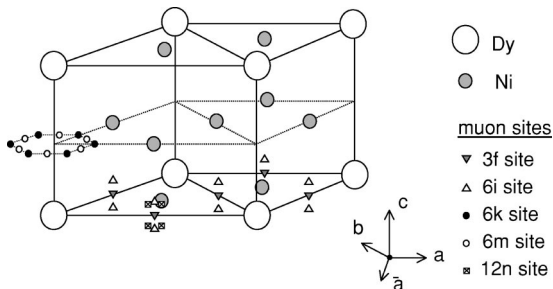
muon site cancel each other. The dipolar coupling tensor $\mathbf{A}_{\text{dip}}$ depends strongly on the coordinates of the muon interstitial site and its experimental determination establishes the muon location site in the compound under study. The trace of the dipolar coupling tensor equals zero.

In the magnetically ordered state of a magnet a spontaneous muon precession frequency is commonly observed. In this case, in the absence of an external field, the precession frequency can be written

$$\omega(T < T_C) = \gamma_\mu \mu_0 \left| \left(\mathbf{A}_{\text{dip}} + \mathbf{A}_{\text{con}} + \frac{1}{3}\mathbf{I} \right) \mathbf{M}_{4f} \right|, \qquad (4)$$

where $\frac{1}{3}\mathbf{I}$ accounts for the Lorentz field and $\mathbf{I}$ is the unit tensor.

IV. RESULTS

A. Muon sites in DyNi₅

All muon spectra have initially been analyzed with

$$aP_X^\alpha(t) = \sum_{i=1}^{n} \sum_{j=1}^{m_i} a_{i,j} \exp(-\lambda_{i,j}^\alpha t) \cos(\omega_{i,j}^\alpha t + \phi), \qquad (5)$$

where n equals the number of crystallographic sites (labeled by i) for the muon and m_i the multiplicity of these sites. a is a parameter depending on the experimental conditions ($a \simeq 0.2$ for the present experiment) and $a_{i,j}$ the initial asymmetry of component i,j. $\Sigma_j a_{i,j}/a$ is therefore the fraction of muons at muon site i. ϕ accounts for the angle between the initial muon spin and the detectors. $\omega_{i,j}^\alpha$ and $\lambda_{i,j}^\alpha$ are, respectively, the average pulsation of precession and the damping rate caused by the depolarization of the muon spin ensemble due to magnetic interactions with its host. They depend on the muon site as well as the orientation α of the external field. In the case of DyNi₅ the total number of observed precession frequencies is either 1, 2, or 3 depending on the orientation of the crystal axes with respect to the external field.

In this section we present the results of the analysis using Eq. (5) over the whole temperature range. We focus here on the determination of the muon sites. We will show that in the temperature range 40–80 K the observed signal is influenced by the presence of the muon in two different crystallographic sites. In this temperature interval, Eq. (5) allows only for an *ad hoc* fit. The proper physical fit will be given in Sec. IV B. In Figs. 2 and 3 the frequency shifts have been plotted as function of the sample susceptibilities for $\mathbf{B}_{\text{ext}} \| c$ and $\mathbf{B}_{\text{ext}} \| a$, respectively. The data points between 40 and 80 K have been omitted from the figures.

First we discuss the results taken with $\mathbf{B}_{\text{ext}} \| c$ presented in Fig. 2. A single signal is observed at all temperatures but at $\chi^c \sim 0.0137$ (corresponding to $T = 80$ K) its frequency shift changes from negative to positive. This indicates that the muon site observed below 80 K is different from the muon site observed above 80 K. The solid lines in Fig. 2 are fits with Eq. (2) for the low- and high-temperature sites, respectively. We find that $K_0 = 0$ for the high temperature site
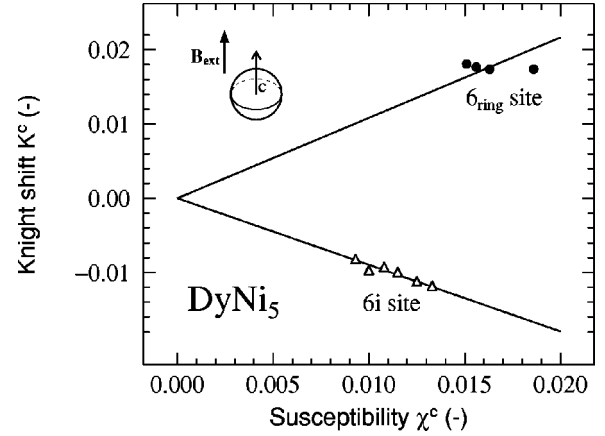

FIG. 2. Frequency shift K^c observed with $\mathbf{B}_{\text{ext}} \| c$ axis plotted as function of the sample susceptibility along that direction. Values in the temperature region between 40 and 80 K have been omitted. Muon precession frequencies are deduced from the μSR spectra with Eq. (5). Two signals are visible, one is observed at high temperature ($\triangle$) the other ($\bullet$) at low temperature. The solid lines are fits with Eq. (2). The slopes of the lines correspond to $A_{\text{dip}}^{cc} + A_{\text{con}}$ for each muon signal. A susceptibility independent Knight shift, as the data of the low temperature site suggest, does not lead to a consistent interpretation of the data.

within experimental error. The deduced coupling tensor elements for the high as well as the low temperature signal are given in Table II.

Figure 4 shows the initial asymmetry and damping rate of the signals plotted as function of temperature. A transition is clearly visible: about half of the total asymmetry is lost below ~ 80 K and the damping rate reaches a maximum at this temperature. Both can be understood if the damping rate of
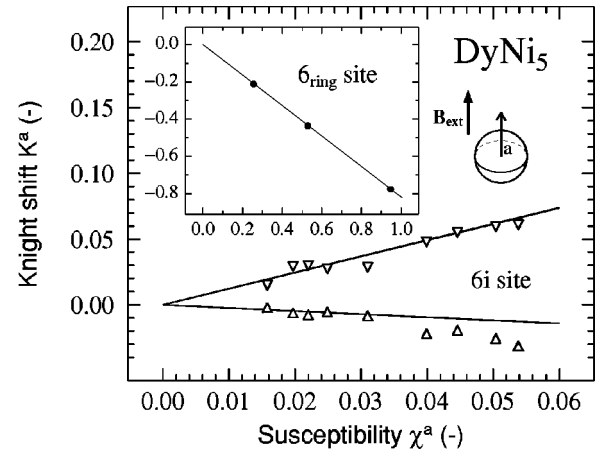

FIG. 3. Same caption as Fig. 2 but data taken with $\mathbf{B}_{\text{ext}} \| a$ axis. The insert shows the full scale, the main graph the details of the high-temperature signals. Three signals are observed, two at high temperature ($\triangle$ and $\triangledown$) the third ($\bullet$) at low temperature. The slopes of the lines corresponds to $A_{\text{dip}}^{aa} + A_{\text{con}}$ for each muon signal. Values in the temperature region between 40 and 80 K have been omitted. The four $\triangle$ at $\chi > 0.035$ have been excluded from the fit as their inclusion lead to inconsistency in determination of the coupling tensor.

TABLE II. Experimental coupling parameters of the muon sites observed in DyNi$_5$ compared to the calculated values. For sites with a multiplicity larger than one, the coupling parameters for the other sites can be obtained via rotation of this coupling tensor. The values for $A_{dip}^{\alpha\alpha}$ of the so-called 6_{ring} site correspond to the average of the respective $A_{dip}^{\alpha\alpha}$ values over the six equivalent $6m$ and $6k$ sites. The experimental values are obtained from the slopes in Figs. 2 and 3. Equation (6) is used to determine $A_{dip}^{\bar{a}\bar{a}}$ of the high-temperature muon site. The angular independent signal in Fig. 6 shows that $A_{dip}^{aa}=A_{dip}^{\bar{a}\bar{a}}$ for the low-temperature site. We identify the low- and high-temperature muon sites as the 6_{ring} and $6i(\frac{1}{2},0,0.1)$ sites.

$\alpha\alpha$	aa	$\bar{a}\bar{a}$	cc
		Experimental	
$T>80$ K, $A_{dip}^{\alpha\alpha}+A_{con}$	1.229(74)	-0.723(69)	-0.897(20)
A_{con}	-0.130(54)	-0.130(54)	-0.130(54)
$A_{dip}^{\alpha\alpha}$	1.359(128)	-0.593(123)	-0.767(74)
$T<80$ K, $A_{dip}^{\alpha\alpha}+A_{con}$	-0.818(16)	-0.818(16)	1.083(47)
A_{con}	-0.184(29)	-0.184(29)	-0.184(29)
$A_{dip}^{\alpha\alpha}$	-0.634(49)	-0.634(49)	1.267(76)
		Calculated $A_{dip}^{\alpha\alpha}$	
$3f$ $(\frac{1}{2},0,0)$	1.558	-0.750	-0.807
$6i$ $(\frac{1}{2},0,0.1)$	1.432	-0.729	-0.702
$6i$ $(\frac{1}{2},0,0.21)$	1.090	-0.668	-0.411
$1b$ $(0,0,\frac{1}{2})$	-1.602	-1.602	3.204
$6j$ $(0.4,0,0)$	2.035	-1.002	-1.032
$12n$ $(0.496,0,0.088)$	1.460	-0.733	-0.725
$2d$ $(\frac{1}{3},\frac{2}{3},\frac{1}{2})$	0.007	0.007	-0.012
$4h$ $(\frac{1}{3},\frac{2}{3},0.2)$	0.214	0.214	-0.427
$6m$ $(0.13,0.26,\frac{1}{2})$	-1.049	-0.263	1.313
$6k$ $(0.225,0,\frac{1}{2})$	-0.263	-1.049	1.313
6_{ring}	-0.656	-0.656	1.313

the high-temperature site increases so much when the temperature approaches 80 K from above that the corresponding precessing signal is no more observed below that temperature. The increase of the damping rate is due to the slowing down of the Dy magnetic moments fluctuations. This is consistent with the increase in zero field damping rate observed between 300 and 100 K.[14] Below 80 K a second site is populated. However the coupling of the muon spin with the Dy moment fluctuations is different from that of the site above 80 K so that the corresponding damping rate remains moderate. This difference in coupling is not surprising since the fluctuations of the Dy moments are expected to be anisotropic. Consequently, although the high-temperature site is still occupied below 80 K, its frequency is not observed because the damping rate is too high ($\lambda_i>40$ MHz) and the signal disappears from the spectrum.

This interpretation is confirmed by the measurements taken with the external field along the a axis. Figure 3 shows two precession signals at high temperature (i.e., low susceptibility) that can be attributed to one muon site, and a single
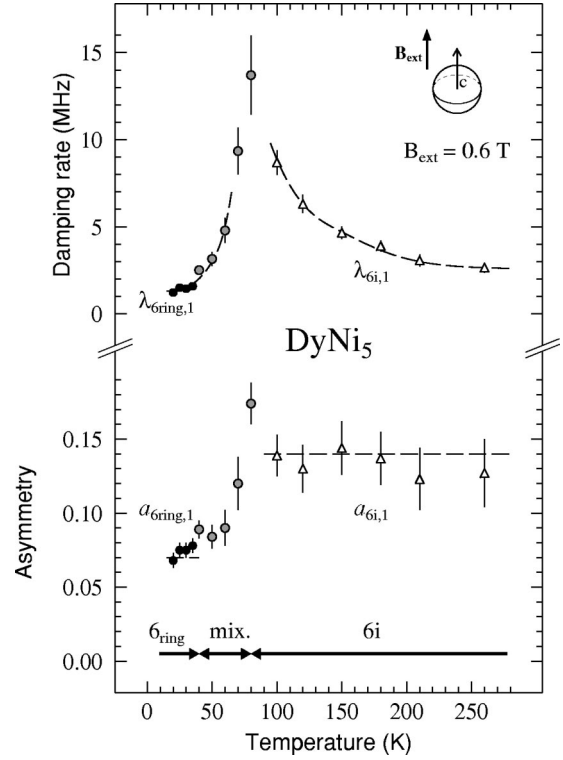

FIG. 4. Initial asymmetry and damping rates of the muon precession signals displayed in Fig. 2. Above 80 K, only site $6i$ is populated. Below 40 K both sites 6_{ring} and $6i$ are populated by the muon but the signal arising from site $6i$ is invisible. The symbol convention is that of Fig. 2. In the temperature range 40–80 K the muon hops from the 6_{ring} to the $6i$ site during its lifetime: the fit with Eq. (5) is an ad hoc fit (gray filled circle symbols). The dashed lines are guides to the eyes. Note that the asymmetry below 40 K is about half of the high-temperature value.

precession frequency at low temperature that originates from a second and different muon site. In Fig. 5 the change in muon site is visible in the damping rates and asymmetries of the signals. At high temperature ($T>80$ K) the asymmetry ratio between the two signals equals 1:2. An angular scan in the $a\bar{a}$ plane has shown that there are in fact three signals of equal asymmetry of which two coincide along the a as well as the $\bar{a}$ axis. Accordingly this muon site has a multiplicity of 3, 6, or 12. If the position vector of the muon site inclines an angle φ with the a axis, a rotation of the dipolar tensor gives

$$A_{dip}^{aa}(\varphi)=A_{dip}^{aa}\cos^2\varphi+A_{dip}^{\bar{a}\bar{a}}\sin^2\varphi. \qquad (6)$$

Here we have set $\chi^a=\chi^{\bar{a}}$ as is the case for DyNi$_5$. We identify the positive coupling in Fig. 3 with $\varphi=0°$ and the negative one with $\varphi=60°$ and $120°$. The deduced values for $A_{dip}^{aa}+A_{con}$ and $A_{dip}^{\bar{a}\bar{a}}+A_{con}$ are given in Table II. The low-temperature site shows a constant single frequency when rotated in the $a\bar{a}$ plane (see Fig. 6) and therefore $A_{dip}^{aa}=A_{dip}^{\bar{a}\bar{a}}$ for this muon site.

The increase in damping rate of the low temperature site above ~30 K indicates that this muon site is unstable. The muon resides for a while at the low temperature site before it
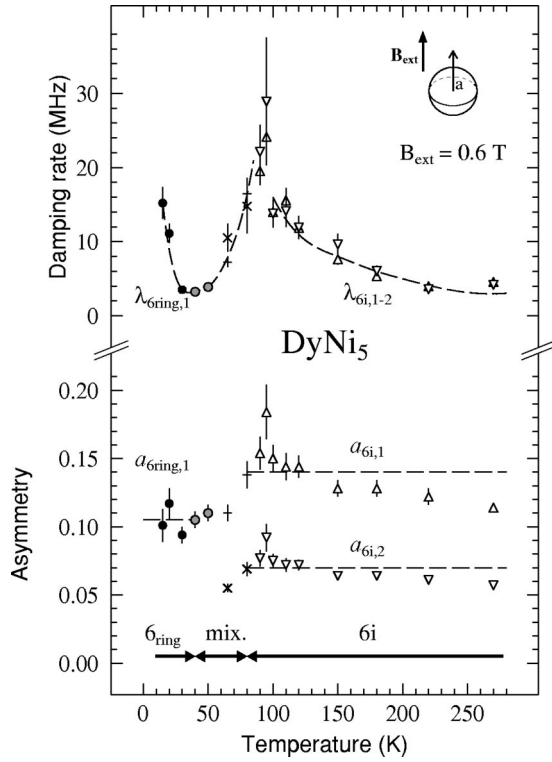
FIG. 5. Initial asymmetry and damping rates of the muon precession signals displayed in Fig. 3. For the temperatures above 60 K where two components are necessary, an initial fit gave the relative values for the asymmetry in the ratio 2:1. The final fit was performed with this ratio fixed. Note that half of the total asymmetry is lost below ~ 50 K. The symbol convention is similar to that of Fig. 3. In addition we have used gray filled circles and + and × symbols for the points where the ad hoc fit requires, respectively, one and two components.

hops to a second preferred muon site. As a consequence the population of the low temperature signal decreases before the muon decays. Since the muon precession signal has been analyzed with Eq. (5) this results in an enhanced damping rate although it reflects a decrease in population. Below 30 K the increase in damping rate (Fig. 5) corresponds to the slowing down of the Dy moments.
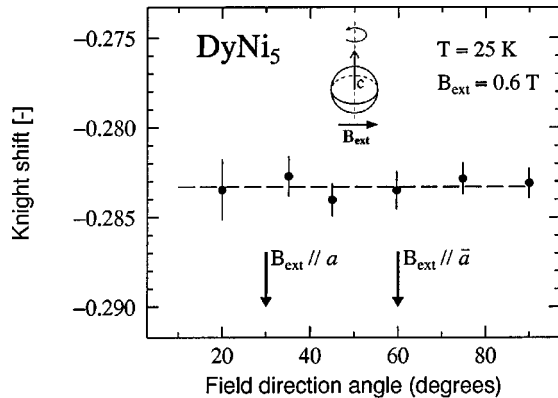

FIG. 6. Frequency shift observed with $\mathbf{B}_{ext}$ aligned in the $a\bar{a}$ plane of the sample at $T=25$ K. The signal shows no angular dependency and $A_{dip}^{aa}=A_{dip}^{\bar{a}\bar{a}}$.
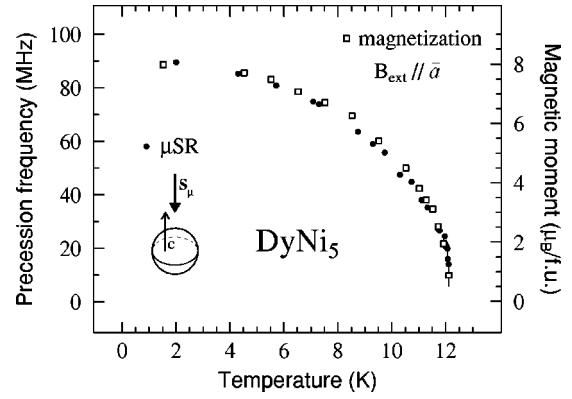

FIG. 7. Spontaneous muon spin precession frequency in DyNi₅ as a function of temperature compared to the spontaneous DyNi₅ moment. The latter has been obtained via linear extrapolation of magnetization curves taken with the external field parallel to $\bar{a}$ and plotted as M^2 vs H/M (Arrot plots). The anisotropy in the $a\bar{a}$ plane is smaller than the lowest field considered and therefore we do not observe the moment reorientation at 6 K. The precession signal of the second muon site is not observed because of its high damping rate.

Zero field measurements performed in the ordered state of DyNi₅ show a single spontaneous precession frequency (Fig. 7). Its temperature dependence is similar to that of the DyNi₅ moment obtained from magnetization curves. Small variations can possibly be attributed to a difference in sensitivity with respect to the Ni moments. Yet, the magnetic order in the Ni sublattice is believed to be induced by the Dy magnetic moments and expected to show the same temperature dependence.

The observation of single muon signal is consistent with the low temperature Knight Shift data and contrasts the results obtained in GdNi₅ where in fact both muon sites are visible.[1] We note that the moment reorientation that occurs in DyNi₅ in the $a\bar{a}$ plane at 6 K (Ref. 12) does not change the muon precession frequency. This is expected for a muon site with axial symmetry ($A_{dip}^{aa}=A_{dip}^{\bar{a}\bar{a}}$). At 2.7 K the precession frequency equals 89.5(3) MHz. The ordered Dy moments are aligned along the $\bar{a}$ axis with a magnitude of 8.9 μ_B (Refs. 8 and 17) and with Eq. (4) we get $A_{dip}^{\bar{a}\bar{a}}+A_{con}=-0.851(2)$ where we have assumed $\mathbf{M}_{4f}$ to be antiparallel to $\mathbf{B}_{loc}$, as usual. This is almost equal to the value that follows from the Knight Shift measurements in the paramagnetic state of the magnet taking into account the experimental error. We note that the experimental uncertainties in the Knight Shift measurements are much larger than those of the measurements in the ordered state. For the latter however the magnitude of the rare earth moment is not always determined accurately.

The hyperfine and dipolar contribution to the coupling between the muon spin and the Dy magnetic moments are separated using the fact that $\mathbf{A}_{dip}$ is a traceless tensor. The experimental values for $A_{dip}^{\alpha\alpha}$ and A_{con} are given in Table II. From the values calculated for different sites we identify the high-temperature site as site $6i$ (1/2,0,0.1). We note that the x and y coordinates of this site are well defined because a small deviation changes the symmetry of this site. Variation

of the z coordinate is possible without altering the symmetry. Consequently there is an uncertainty in the determination of z coordinate of the $6i$ site.

The low-temperature site shows uniaxial symmetry. The interstitial sites with such a symmetry $(0,0,x)$ and $(1/3,2/3,x)$ show a strong and a weak dipolar coupling with the Dy moments respectively. The experimental value is in between those values and the low-temperature muon site cannot be identified as such.

The dipolar coupling A_{dip}^{cc} for the $6m$ and $6k$ sites corresponds to the experimental value. However, muons located at one of these two sites, give rise to three frequencies in Fig. 6. If the muon on the other hand occupies all six ring sites within the time scale of the experiment, an average is obtained that shows axial symmetry. The experimental values for A_{dip}^{aa} and $A_{\text{dip}}^{\overline{aa}}$ correspond to this average. As in GdNi$_5$ (Ref. 1) we identify the low-temperature site as the 6_{ring} site.

Both 6_{ring} and $6i$ sites are approximately equally populated below 50 K. This is shown by the loss of a factor ~ 2 in the total asymmetry at low temperature compared to its high-temperature value (see Figs. 4 and 5). The 6_{ring} site is identical to the low temperature site observed in GdNi$_5$. The $6i$ site is localized just above or below the $3f$ site which is the stable site in GdNi$_5$ (see Fig. 1).

As the distance between two adjacent $6i$ sites (along the c axis) is small, in fact smaller than the distance between two adjacent 6_{ring} sites, it is likely that the muon hops between two $6i$ sites at high speed (or forms a delocalized dumbbell state) just as it does at the 6_{ring} site. Experimentally we can

not distinguish if the muon is localized at a single $6i$ site, if it hops between two $6i$ sites or if it forms a dumbbell state.

In LaNi$_5$ the $12n$ site is one of the H location sites and recent first principle calculations identify this site as the most favorable.[18] Table II shows that the coupling parameters of the $12n$ site do correspond to the experimental values of the high-temperature muon site. If the muon resides at the $12n$ site it can be expected that it simultaneously occupies neighboring sites at each side of the $6i$ site, as they are only 0.04 Å apart. We cannot exclude that the muon occupies the $12n$ site instead of the $6i$ site but the observed asymmetry ratio of 1:1 suggests an equal multiplicity of both sites. On the other hand, the possibility exists that the low-temperature ring site consists of both the $6m$ and $6k$ site and forms a ring of 12 sites. This contradicts the results on GdNi$_5$ where a asymmetry ratio of 2:1 has been observed between the 6_{ring} site and the $3f$ site. We therefore conclude the $6i$ site is the most likely.

B. Muon hopping in DyNi$_5$

Analysis with a simple exponential muon depolarization [Eq. (5)] fails to describe the muon polarization signal around 80 K as the hopping muon sees two different environments during its lifetime. The average residence time of the muons at the 6_{ring} site τ_{ring} has to be taken into account. Hence the TF μSR spectra taken around 80 K have been analyzed with the following depolarisation function corresponding to the generalization of the model of Ref. 19:

$$aP_X(t)=\sum_{j=1}^{m_i} a_{6i,j}\exp(-\lambda_{6i,j}t)\cos(\omega_{6i,j}t)+a_{\text{ring}}\left\{\exp(-\lambda'_{\text{ring}}t)\cos(\omega_{\text{ring}}t)\right.$$

$$\left.+\frac{\exp(-\lambda_{6i,j}t)\cos(\omega_{6i,j}t+\theta_m)\;-\;\exp(-\lambda'_{\text{ring}}t)\cos(\omega_{\text{ring}}t+\theta_m)}{\tau_{\text{ring}}\sqrt{(\lambda'_{\text{ring}}-\lambda_{6i,j})^2+4(\delta\omega)^2}}\right\} \tag{7}$$

with

$$\lambda'_{\text{ring}}=\lambda_{\text{ring}}+\frac{1}{\tau_{\text{ring}}}, \quad \delta\omega=\frac{\omega_{\text{ring}}-\omega_{6i,j}}{2}, \quad \text{and}$$

$$\tan\theta_m=\frac{2\delta\omega}{\lambda'_{\text{ring}}-\lambda_{6i,j}}.$$

For convenience the index α for the orientation of the external field has been dropped. m_i equals 2 for $\alpha=a$ and 1 for $\alpha=c$. Our focus in this section is the determination of τ_{ring} because its temperature dependence will give information about the mechanism governing the muon hopping.

As the damping rate of the $6i$ site increases rapidly below 100 K and the $6i$ signal becomes difficult to observe, the fits are not sensitive to τ_{ring} but mainly to $\lambda'_{\text{ring}}=\lambda_{\text{ring}}+1/\tau_{\text{ring}}$.

We introduce $\tau'_{\text{ring}}=1/\lambda'_{\text{ring}}$ which is plotted as function of $1/T$ in Fig. 8. Recalling the rapid increase of the damping rate of the $6i$ site below 100 K as well as that of the 6_{ring} site below 30 K (Fig. 5) we infer that $\lambda_{\text{ring}}^\alpha$ must be small and close to zero at 80 K. Therefore, in the high temperature limit of the hopping region we have $\tau'_{\text{ring}}=\tau_{\text{ring}}$. In the low-temperature limit $\lambda'_{\text{ring}}\rightarrow\lambda_{\text{ring}}$ as the residence time at the ring site exceeds the time of the μSR experiment.

The solid line in Fig. 8 describes the residence time of the muon at the 6_{ring} site as function of temperature assuming multiphonon induced muon tunneling to the $6i$ site. Multiphonon processes equalize for an extremely short time (of the order of 10^{-13} s) the local energy levels of the potential well where the muon is localized and where it likes to jump. When this occurs the muon can tunnel through the energy barrier between the two sites. Within the framework of the small polaron theory[20,21]
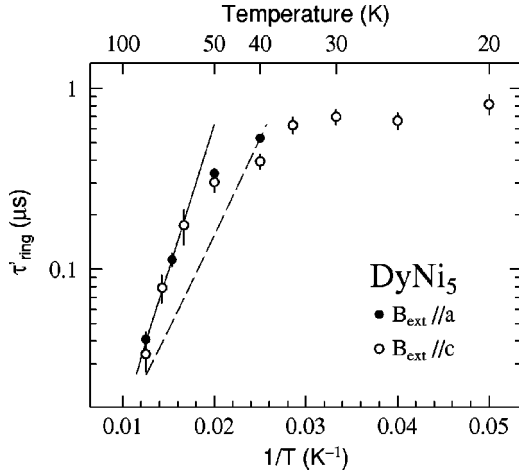
FIG. 8. $\tau'_{\text{ring}} = 1/\lambda'_{\text{ring}}$ as deduced with Eq. (7) from the spectra taken in the transition region. At high temperature (60 K$<T$ $<$80 K) $\lambda_{\text{ring}} \approx 0$ and $\tau_{\text{ring}} = \tau'_{\text{ring}}$. At lower temperature the critical slowing down of the Dy moments dominates ($\lambda_{\text{ring}} = 1/\tau'_{\text{ring}}$). The full line is the result of a fit with Eq. (8), $E_a/k_B = 400$ (20) K and $J = 0.21$ (7) meV. For comparison the residence time at the 6_{ring} site in GdNi$_5$ is shown with a dashed line.

$$\tau_{\text{ring}} = \frac{\hbar}{J^2} \sqrt{\frac{4 E_a k_B T}{\pi}} \exp\left(\frac{E_a}{k_B T}\right), \qquad (8)$$

where E_a is the coincidence energy needed to equalize the energy levels of both potential wells and J the tunneling matrix element (Fermi's golden rule). We get E_a/k_B $=400(20)$ K and $J=0.21(7)$ meV. If the minimum damping rate of the ring site equals 1 μs^{-1} instead of zero, a reduction in both E_a and J of a few percent is obtained.

A comparison of these values with the results obtained on GdNi$_5$ [$E_a/k_B = 272(10)$ K and $J = 0.11(2)$ meV, dotted line in Fig. 8] is given in Fig. 9. The potential well of the $6i$ site is deeper with respect to the 6_{ring} site than the potential well at the $3f$ site is. In this figure we have assumed that the 6_{ring} environment is similar in both compounds. This is not necessarily the case. The tunneling matrix element J is larger

in DyNi$_5$ consistent with the smaller distance between 6_{ring} and $6i$ site (2.07 Å) compared to the distance between 6_{ring} and $3f$ site (2.39 Å).

C. Muon sites in RNi$_5$

For TbNi$_5$ a spontaneous precession frequency of 79.2 MHz has been reported at 4.2 K.[11] In the latter compound the Tb moments show planar ferromagnetism with moments of $7.9\mu_B$ along the a axis. We deduce $A_{\text{dip}}^{aa} + A_{\text{con}} = -0.850$. Comparing this with DyNi$_5$ and taking into account that the coupling of the muon spin at the 6_{ring} site with the rare earth moments is isotropic in the $a\bar{a}$ plane, it is reasonable to suggest that the 6_{ring} site is also occupied at low temperature in TbNi$_5$.

In paramagnetic LaNi$_5$ (Ref. 9) the $3f$ site has been reported as the location site of the muon. We note that the $6i$ site as the most preferred site cannot be excluded for the following reason. The experimentally observed value for the depolarization due to the nuclear moments equals 0.100(2) MHz whereas we calculate for the $6i$ $(1/2,0,0.21)$ site a value of 0.097 MHz. For the $3f$ site this is 0.105 MHz. The lattice parameters as listed in Table I have been used in this calculation.

Also in ErNi$_5$ the $3f$ site has been reported as the most likely muon location site.[8] Crystal field effects are prominent in this compound and the determination of the muon site has been ambiguous. Therefore, when looking for a systematic trend in muon location behavior in Sec. V, we focus on PrNi$_5$, DyNi$_5$, and GdNi$_5$.

V. DISCUSSION

In PrNi$_5$ the muon localizes at the $6i$ $(1/2,0,0.21)$ site and the 6_{ring} site is not observed $(T>4$ K).[10] It is remarkable that going from Gd- to Dy- to PrNi$_5$ the stable muon site moves from $3f$ to $6i$ $(1/2,0,0.1)$ to $6i$ $(1/2,0,0.21)$. We note that if the $12n$ site is the preferred site in DyNi$_5$, this results in a similar trend. This trend does not follow the lattice parameters nor is it correlated to the charge of the nucleus as
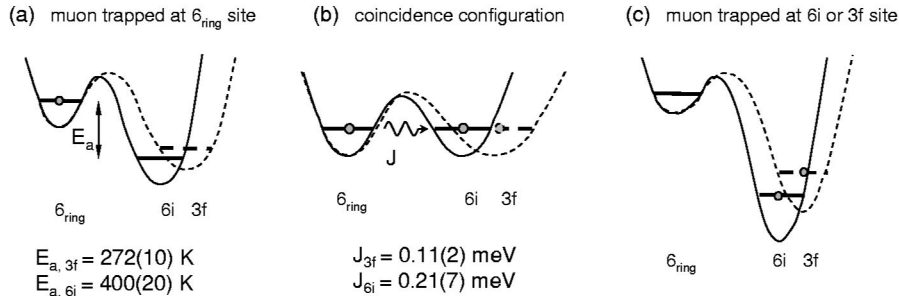

FIG. 9. Impression of the muon potential wells in GdNi$_5$ and DyNi$_5$. The 6_{ring} site has been observed in both compounds at low temperature whereas the $3f$ and $6i$ sites are the stable sites in both compounds, respectively. From the μSR spectra the coincidence energy E_a and the tunneling matrix element J have been deduced leading to the energy level scheme at low temperature (a) and the coincidence configuration (b). The distance between 6_{ring} and $6i$ equals 2.07 Å and the distance between 6_{ring} and $3f$ equals 2.39 Å. Note that the muon deforms the lattice locally thereby creating a self-trapped state. At (a) the muon is localized at the 6_{ring} site. At (b) the tunneling transition from 6_{ring} to $6i$ or $3f$ can occur. After this tunneling process the muon becomes self-trapped at the $6i$ or $3f$ and the energy difference between the 6_{ring} and $6i$ or $3f$ is much larger than E_a preventing muon transport in the opposite direction.
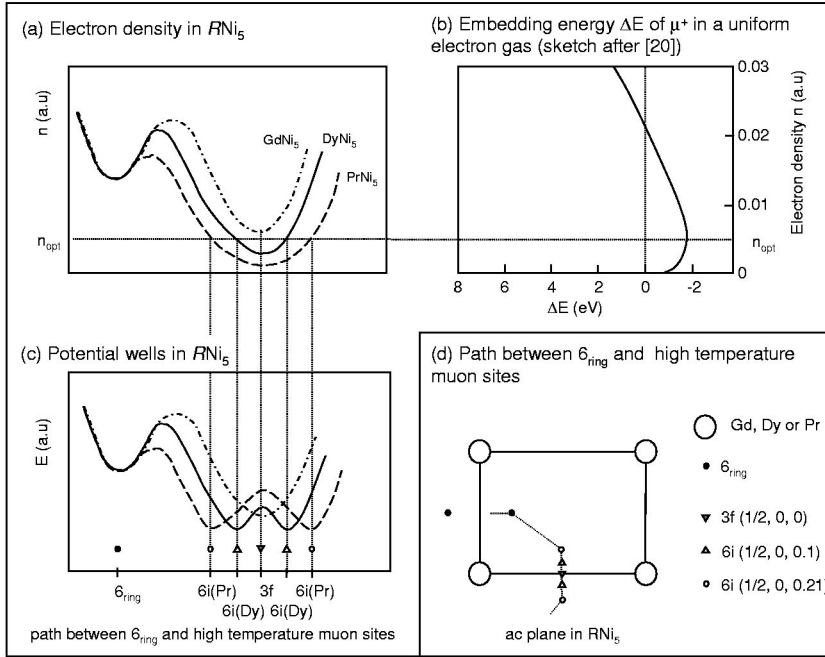
FIG. 10. Possible mechanism for the variation of muon sites in RNi$_5$. Here we assume the electron density at the 6_{ring} site is constant. Due to a minimum in embedding energy (b) there is an optimum electron density for muon localization n_{opt} (Ref. 23). A lowering of the electron density around the $3f$ site (a) below n_{opt} shifts the preferred muon site to the $6i$ site (c). The reduced distance and reduced energy barrier between 6_{ring} and $6i$ (1/2,0,0.21) in PrNi$_5$ prevent the muon from localizing at the first site. The difference in electron density through the RNi$_5$ series has been exaggerated in (a) for clarity of the figure. (d) shows the path set out along the horizontal axis of (a) and (b).

can be seen in Table I. The fact that either the $6i$ or $3f$ site are observed in similar compounds seems to suggest that the undisturbed surroundings of the $3f$ site are similar to a potential lake, it is nearly flat and without deep minima. Small differences can make the muon localize at either the $3f$ or $6i$ site. We note that the $6i$ (1/2,0,0.1) site has maximum distance to its nearest Ni neighbors. For the $3f$ site the in plane Ni neighbors are closer whereas for the $6i$ (1/2,0,0.21) site the (1/2,0,1/2) Ni atom is closest.

The 6_{ring} site is not observed in PrNi$_5$ and this could have two origins. Either the environment of the 6_{ring} is such that the muon does not become trapped or alternatively the transition from the 6_{ring} to the $6i$ (1/2,0,0.21) site is too fast to be observed and a small coincidence energy and/or large tunneling matrix element is expected. To give an idea of the quantities involved, we estimate from Eq. (8) with τ_{ring} <0.01 μs and $T=4$ K that $E_a/k_B < 75$ K for $J=100$ meV and $E_a/k_B < 26$ K for $J=0.2$ meV.

An optimum electron density has been calculated for a proton embedded in an electron gas with an homogeneous electron density.[22] This theory depends on the charge of the proton only and a muon is expected to behave similarly. Generally, for muons in metallic hosts, the electron density exceeds this optimum and the muon prefers the interstitial site with the lowest electron density.[23] The shift in muon location site from $3f$ to $6i$ can be understood if the electron density at the $3f$ site in DyNi$_5$ is lower than the optimum electron density. In this case the optimum could be found just beside the $3f$ site, i.e., at the $6i$ site. The higher coincidence energy also hints to an increase in stability for the $6i$ site. The variety in muon sites in isostructural compounds is large[3] and if the electron density in these lattices varies around an optimum value, a change in host atoms or lattice parameters could readily alter the most favorable interstitial site for the muon. A comparison of GdNi$_5$ and YNi$_5$ with

various other Gd and Y-Ni compounds suggest indeed that the density of states (DOS) at the Fermi level is a minimum for RNi$_5$.[24]

The change in z coordinate of the stable muon site from 0.21 to 0.1 to 0 in the Pr-Dy-GdNi$_5$ series suggests some form of a structural development or mechanism that influences the muon location site beyond hole size and simple electronic configuration considerations. The prediction of muon sites has been a difficult task in the past and this study certainly confirms this. At the moment we can only speculate and notice that there seems to be a correlation between the magnetic moment of the Ni atoms and the reduction in z coordinate of the muon location site (see Table I). The contribution of the Ni $3d$ electrons to the DOS at the Fermi level is substantial in PrNi$_5$ (Ref. 25 and 26) and therefore it is expected that these electrons play an important role in the muon localization. In contrast to this the rare earth $4f$ electrons are typically localized within the electron cloud surrounding the rare earth nucleus. A recent magnetic circular dichroism study on GdNi$_5$ and TbNi$_5$ shows a strong influence of the rare earth magnetic moment on the Ni K edge in the dichroic spectra[27] confirming the Ni moment is induced by the rare earth moments. This moment induction is expected to follow the de Gennes scaling and is largest for GdNi$_5$. Clearly, this phenomenon takes place below the magnetic ordering temperature whereas the muon location exists at room temperature and there is no static moment on the Ni atoms in this temperature regime. However it is a measure for the interaction between the $4f$ and $3d$ electrons and this study seems to suggest that interaction between these electrons is of significance for the muon localization, even at room temperature. Recent calculations on a cluster resembling RNi$_5$ also shows a strong interaction between the Ni $3d$ orbit and the R $4f$ orbit.[28] A comparison of electronic band structure calculations for the various RNi$_5$ compounds

would be interesting but to our knowledge such calculations have not been performed.

In Fig. 10 we summarize a possible explanation for the muon location behavior in Pr-, Dy-, and GdNi$_5$. A diminishing interaction between the R-$4f$ and Ni-$3d$ electrons reduces the local electron density around the $3f$ site and causes the optimum electron density for muon localization and thus the preferred muon site, to move from the center to the $6i$ sites. The smaller distance and reduced energy barrier between the 6_{ring} and the $6i$ site in PrNi$_5$ prevents the muon becoming trapped at the former site. From Fig. 10(b) and the difference in E_a (Fig. 9) we estimate that a change in electron density of about 20% is needed to explain the change in muon site. In the case the electron density is not near the optimum electron density but at higher values, a change of about 0.5 to 1 % explains the difference in E_a.

The DOS of the $3d$ electrons in PrNi$_5$ (Ref. 25) has been measured, but there are no detailed studies of the other RNi$_5$. Recent calculations show a sharp high DOS of the $3d$ electrons at the Fermi level in RNi$_5$[28] but this is in contrast with the previous mentioned experimental results. Band structure calculations for YNi$_5$, LaNi$_5$, and CeNi$_5$ (Ref. 29) show that there is an increase in the DOS at the Fermi level when the lattice constant decreases along this series.

Recent first principles calculations of hydrogen absorption in LaNi$_5$ (Ref. 18) show progress in predicting the preferred site for the hydrogen. In a double unit cell the atoms are allowed to relax and it is shown that this is a significant criteria for H localization. The authors emphasize the importance of the Ni-H bond and the significance of the distance between the Ni and H. It confirms the Ni $3d$ electrons play a major role in the electronic structure of La$_2$Ni$_{10}$H. It would be interesting to include the 4f electrons in this calculation to see if it predicts a change of the stable site towards the $3f$ site with rare earth substitution.

In PrNi$_5$ an influence of the muon on the crystal field surrounding the neighboring Pr atoms has been observed.[10] It

manifests itself in a deviation of the linear relation between the Knight Shift and the bulk susceptibility since the local susceptibility at the muon site is altered. In DyNi$_5$ we do not observe these effects. The crystal field levels of the Dy ion are all doublets[8] and remain doublets under the distortion of the muon. Possibly the distance between the crystal field levels and their eigenfunctions change but the effect on the susceptibility is small. The crystal field levels in PrNi$_5$ are singlets and doublets, of which some of the latter loose their degeneracy due to the muon presence. In this case the effect of the muon on its surroundings is significant enough to be observed.

VI. CONCLUSION

In this paper we have determined the muon sites in DyNi$_5$. At low temperature the muon occupies both the 6_{ring} site and the $6i$ (1/2,0,0.1) site. The first site is metastable. At low temperature the muon remains at the 6_{ring} site during its lifetime and at higher temperature it only occupies the $6i$ site. In the temperature region in between $(60\,K < 80\,K)$ we clearly observe that the muon hops from the 6_{ring} to the $6i$ site during its lifetime. We have determined the mean lifetime at the 6_{ring} site and analyzed its temperature dependence with multiphonon assisted tunneling $[E_a/k_B = 400(20)\,K$ and $J = 0.21\,(7)\,meV]$.

A comparison of the muon hopping in GdNi$_5$ and DyNi$_5$ gives insight in localization behavior and a assessment of coincidence energies suggests that the $6i$ site in DyNi$_5$ is more favorable than the $3f$ site in GdNi$_5$. The large variety in reported muon sites can be understood if the electron density at the Fermi level is relatively low in these materials and close to the optimum value for muon localization. In this case small changes in electronic structure can have large effects on the muon location behavior. An additional factor in the muon location behavior is possibly the interaction between the rare earth $4f$ and the Ni $3d$ electrons which might increase the $3d$ electron density at the Fermi level.

[1] A. M. Mulders, Ph.D. thesis, Delft University of Technology, 1998, Chap. 6.

[2] A.M. Mulders, C.T. Kaiser, P.C.M. Gubbens, A. Amato, F.N. Gygax, M. Pinkpank, A. Schenck, P. Dalmas de Réotier, A. Yaouanc, K.H.J. Buschow, F. Kayzel, and A. Menovsky, Physica B **289-290**, 451 (2000).

[3] A.M. Mulders, P.C.M. Gubbens, C.T. Kaiser, A. Amato, F.N. Gygax, A. Schenck, P. Dalmas de Réotier, A. Yaouanc, K.H.J. Buschow, F. Kayzel, and A.A. Menovsky, J. Alloys Compd. **330-332**, 454 (2002).

[4] A. Schenck, N.K. Sato, G. Solt, D. Andreica, F.N. Gygax, M. Pinkpank, and A. Amato, Eur. Phys. J. B **13**, 245 (2000); A. Amato, D. Andreica, F.N. Gygax, M. Pinkpank, N.K. Sato, A. Schenck, and G. Solt, Physica B **289-290**, 447 (2000).

[5] Ch. Niedermayer, C. Bernhard, T. Holden, R.K. Kremer, and K. Ahn, Phys. Rev. B **65**, 094512 (2002).

[6] A. Schenck, D. Andreica, F.N. Gygax, and H.R. Ott, Phys. Rev. B **65**, 024444 (2001).

[7] K.H.J. Buschow, Rep. Prog. Phys. **40**, 1179 (1977).

[8] F. E. Kayzel, Ph.D. thesis, University of Amsterdam, 1996, pp. 90–96.

[9] P. Dalmas de Réotier, Ph.D. thesis, Institut National Polytechnique de Grenoble, 1990.

[10] R. Feyerherm, A. Amato, A. Grayevsky, F.N. Gygax, N. Kaplan, and A. Schenck, Z. Phys. B: Condens. Matter **99**, 3 (1995).

[11] P. Dalmas de Réotier, J.P. Sanchez, A. Yaouanc, S.W. Harris, O. Hartmann, E. Karlsson, R. Wäppling, D. Gignoux, B. Gorges, D. Schmitt, Ph. L'Héritier, A. Weidinger, and P.C.M. Gubbens, Hyperfine Interact. **64**, 389 (1990).

[12] G. Aubert, D. Gignoux, B. Michelutti, and A. Naït-Saada, J. Magn. Magn. Mater. **15-18**, 551 (1980).

[13] G. Aubert, D. Gignoux, B. Hennion, B. Michelutti, and A. Naït-Saada, Solid State Commun. **37**, 741 (1981).

[14] P. C. M. Gubbens, A. A. Moolenaar, P. Dalmas de Réotier, A. Yaouanc, F. Kayzel, J. J. M. Franse, K. Prokes, C. E. Snel, P. Bonville, J. A. Hodges, and P. Imbert (unpublished).

[15] P. Dalmas de Réotier and A. Yaouanc, J. Phys.: Condens. Matter **9**, 9113 (1997).

[16] A. Schenck, in *Muon Science, Muons in Physics, Chemistry and Materials*, edited by S. L. Lee, S. H. Kilcoyne, and R. Cywinski (IoP Publishing, Bristol, 1998).

[17] P.C.M. Gubbens, A.M. van der Kraan, and K.H.J. Buschow, Phys. Rev. B **39**, 12 548 (1989).

[18] K. Tatsumi, I. Tanaka, H. Inui, K. Tanaka, M. Yamaguchi, and H. Adachi, Phys. Rev. B **64**, 184105 (2001).

[19] A. Möslang, H. Graf, G. Balzer, E. Recknagel, A. Weidinger, Th. Wichert, and R.I. Grynszpan, Phys. Rev. B **27**, 2674 (1983).

[20] C.P. Flynn and A.M. Stoneham, Phys. Rev. B **1**, 3966 (1970).

[21] V.G. Storchak and N.V. Prokof'ev, Rev. Mod. Phys. **70**, 929 (1998).

[22] M.J. Puska, R.M. Nieminen, and M. Manninen, Phys. Rev. B **24**, 3037 (1981).

[23] E. B. Karlsson, *Solid State Phenomena as Seen by Muons, Protons, and Excited Nuclei* (Clarendon Press, Oxford, 1995).

[24] D. Gignoux, D. Givord, and A. Del Moral, Solid State Commun. **19**, 891 (1976).

[25] K. Krug, K. Winzer, M. Reiffers, J. Kunes, P. Novák, and F. Kayzel, Eur. Phys. J. B **18**, 595 (2000).

[26] S.K. Malik, F.J. Arlinghaus, and W.E. Wallace, Phys. Rev. B **25**, 6488 (1982).

[27] R.M. Galéra and A. Rogalev, J. Appl. Phys. **85**, 4889 (1999).

[28] G. Jin and H. Li, J. Phys. Chem. Solids **62**, 2055 (2001).

[29] L. Nordström, M.S.S. Brooks, and B. Johansson, Phys. Rev. B **46**, 3458 (1992).